

## Article

# Anti-Photoaging Effect of Jawoongo via Regulating Nrf2/ARE and TGF- $\beta$ /Smad Signaling in In Vitro Photoaging Model

Hongyong Kim <sup>1,†</sup>, Qiwen Zheng <sup>1,†</sup>, Sarang Oh <sup>1,2</sup> , Shengdao Zheng <sup>1,2</sup>, Myeongju Kim <sup>1</sup> and Tae-Hoo Yi <sup>1,\*</sup> 

<sup>1</sup> Graduate School of Biotechnology, Kyung Hee University, 1732 Deogyong-daero, Giheung-gu, Yongin-si 17104, Republic of Korea; junoenc73@khu.ac.kr (H.K.); zhengqiwen@khu.ac.kr (Q.Z.); blazma1021@kmu.kr (S.O.); sdjeong0719@khu.ac.kr (S.Z.); espritmj@khu.ac.kr (M.K.)

<sup>2</sup> Snowwhitefactory Co., Ltd., 807 Nonhyeon-ro, Gangnam-gu, Seoul 06032, Republic of Korea

\* Correspondence: drhoo@khu.ac.kr; Tel.: +82-31-201-3693

† These authors contributed equally to this work.

**Abstract:** Jawoongo is a traditional prescription used widely in East Asia for external applications and is effective for burns, sunburn, wounds, and symptoms of dryness in skin disease. This study was established to examine how Jawoongo treatment affects the photodamage of HaCaT cells caused by ultraviolet B (UVB) irradiation and explore its possible anti-photoaging mechanisms from the perspective of the associated signaling pathways. An in vitro photoaging model was established by irradiating HaCaT with UVB, and the expression of photodamage markers such as matrix metalloproteinases (MMPs) and reactive oxygen species (ROS) was assessed by enzyme-linked immunosorbent assay (ELISA), FACs, and RT-PCR. Western blotting was also used to ascertain the expression levels of the TGF- $\beta$ /Smad and nuclear erythroid 2-related factor (Nrf2)/antioxidant response element (ARE) signaling pathways. The findings of this study showed that the increased production of ROS, MMP-1, and MMP-3 due to UVB irradiation was reduced by Jawoongo. In addition, the Nrf2/ARE and TGF- $\beta$ /Smad pathways were upregulated by Jawoongo, while it reduced phosphorylation activation of the mitogen-activated protein kinase (MAPK)/activator protein 1 (AP-1) pathway. This study shows that Jawoongo regulates the Nrf2/ARE and TGF- $\beta$ /Smad signaling pathways in UVB-irradiated HaCaT cells, highlighting its potential to protect against and repair skin photodamage.

**Keywords:** Jawoongo; anti-photoaging; ultraviolet B (UVB); Nrf2/ARE; TGF- $\beta$ /Smad



**Citation:** Kim, H.; Zheng, Q.; Oh, S.; Zheng, S.; Kim, M.; Yi, T.-H. Anti-Photoaging Effect of Jawoongo via Regulating Nrf2/ARE and TGF- $\beta$ /Smad Signaling in In Vitro Photoaging Model. *Appl. Sci.* **2023**, *13*, 10425. <https://doi.org/10.3390/app131810425>

Academic Editor: Marco G. Alves

Received: 29 August 2023

Revised: 14 September 2023

Accepted: 15 September 2023

Published: 18 September 2023



**Copyright:** © 2023 by the authors. Licensee MDPI, Basel, Switzerland. This article is an open access article distributed under the terms and conditions of the Creative Commons Attribution (CC BY) license (<https://creativecommons.org/licenses/by/4.0/>).

## 1. Introduction

The different forms of ultraviolet (UV) radiation, namely, UVA, UVB, and UVC, have varying impacts on the skin depending on their wavelength. Among them, UVB has the most biological activity and is most absorbed by DNA, so it is often considered the main factor behind UV-induced diseases [1,2]. It mainly acts on the epidermis and extracellular matrix (ECM) by interacting with chromophores and photosensitizers [3,4].

Reactive oxygen species (ROS) produced in excess due to UVB irradiation are the primary mediators behind the activation of various oxidative stress pathways [5]. Excessive ROS causes oxidative damage to crucial biomacromolecules (e.g., proteins, lipids, and nucleic acids) in cells and induces mitochondrial DNA damage, apoptosis, and cell cycle arrest [6,7]. They further upregulate matrix metalloproteinases (MMPs) through pathways such as mitogen-activated protein kinase (MAPK)/activator protein 1 (AP-1) and decompose the ECM, which decreases the strength and elasticity of the skin [8]. Deep wrinkles, inelasticity, and non-healing ulcers caused by the degradation of elastin and collagen fibers in the ECM are the most intuitive manifestations of skin photoaging.

Many studies have shown that plant supplements can cut oxidative free radicals from hemoglobin and regulate collagen production by upregulating the nuclear erythroid 2-related factor (Nrf2)/antioxidant response element (ARE) natural antioxidant pathway

and the transforming growth factor (TGF)- $\beta$ /Smad collagen synthesis pathway [9,10]. Nrf2 is transferred from the cytosol to the nucleus to activate ARE-dependent genes and promote the production of antioxidant enzymes such as NAD(P)H quinone oxidoreductase-1 (NQO1), dihydrolipoamide dehydrogenase (DLD), and heme oxygenase-1 (HO-1) to remove harmful quinones and relieve oxidative stress [11]. The expression of TGF- $\beta$  is mediated by the Smad protein family [12]. Inhibitory Smads (Smad6 and Smad7) can bind to TGF- $\beta$  receptors [13] and impede the ability of R-Smad (Smad2 and Smad3) to interact with TGF- $\beta$  receptors to block the expression of procollagen genes [14]. In this way, the damaged cell structure and function caused by high ROS can be restored to achieve anti-photoaging effects.

Jawoongo (JAUN) is a traditional ointment commonly used in China, Japan, and Korea for inflammatory diseases of the skin, dry and keratinizing diseases, burns, trauma, abnormal pigmentation, and the prevention and healing of wounds. It is primarily composed of *Lithospermum erythrorhizon* and *Angelica gigas*, with addition and reduction. The *Lithospermum erythrorhizon*-derived active components of JAUN include naphthoquinone compounds, such as shikonin derivatives, which have been demonstrated to have anti-inflammatory, antibacterial, and antitumor effects, as well as being able to scavenge ROS [15,16]. In terms of the *Angelica gigas*-derived active ingredients, these include decursin, decursinol angelate, and nodakenin, which have been reported to have therapeutic effects against allergy-related inflammation, as well as anti-cancer and anti-depression activities [17,18]. The pharmacological properties of JAUN have been substantiated through in vitro and in vivo experiments regarding its ability to prevent atopic dermatitis and promote wound healing [19,20]. Nevertheless, to the best of our knowledge, no reports on the anti-photoaging properties of JAUN have been published.

This study was implemented to investigate the activity and mechanisms of action of the JAUN-modified formula on HaCaT cells induced by UVB photoaging. In addition, the anti-photoaging effects of JAUN were investigated by analyzing the levels of MMPs, ROS, and procollagen type I as well as the expression levels of the TGF- $\beta$ /Smad and Nrf2/ARE signaling pathways, which are key regulatory biomarkers of skin photoaging.

## 2. Materials and Methods

### 2.1. Materials

Human keratinocytes (HaCaT) were purchased from ATCC (Manassas, VA, USA). The fetal bovine serum (FBS), DMEM, antibiotic/antifungal solution, and ECL reagents were provided by Hyclone (Waltham, MA, USA). Additionally, 0.25% trypsin EDTA, 4,5-dimethylthiazol-2-yl-2,5-diphenyltetrazolium bromide (MTT), radioimmunoprecipitation assay (RIPA) buffer, 1,1-diphenyl-2-picrylhydrazyl (DPPH), and 2',7'-dichlorofluorescein diacetate (DCFH-DA) were bought from Gibco (Grand Island, NY, USA) and Sigma Chemical (St. Louis, MO, USA). TRIzol reagent, PCR premix, and nucleic acid staining were obtained from Life Technologies Corporation (Carlsbad, CA, USA), Bioneer (Daejeon, Republic of Korea), and NobleBio (Gyeonggi, Republic of Korea), respectively. The primary and secondary antibodies were secured from Santa Cruz Biotechnology (Santa Cruz, CA, USA), Cell Signaling Technology (Beverly, MA, USA), Bio-Rad Laboratories, Inc. (Hercules, CA, USA), and Proteintech Group, Inc. (Rosemont, IL, USA). All other materials used were purchased from commercial sources in the highest grades available and were used as received without any further purification.

### 2.2. Sample Preparation

A total of 13 medicinal materials were used to produce JAUN, namely, made in China and Korea *Lithospermum erythrorhizon* roots, *Angelica gigas* roots, *Ulmus davidiana* roots, *Sophora flavescens* roots, *Scutellaria baicalensis* roots, *Glycyrrhiza glabra* roots, *Lonicera japonica* flower, *Forsythia koreana* fruits, *Hibiscus syriacus* roots, *Chrysanthemum indicum* flower, *Paeonia lactiflora* bark, *Poncirus trifoliata* fruits, and *Angelica dahurica* roots, were purchased from Dongkwang Corporation (Seoul, Republic of Korea). A total of 130 g of a

mixture of all 13 medicinal materials (10 g of each) mentioned above was extracted with 1300 mL of a 70% ethanol solution. Then, 24 h after that, the mixture was filtered and lyophilized. The yield of the final JAUN extract was 19.23% (*w/w*), and the Global Campus of Kyung Hee University (Voucher Specimen NO: QBDC2023-023, Yongin, Gyeonggi, Republic of Korea) preserved the voucher specimen for safekeeping.

### 2.3. Phenolics and Flavonoids Content Assay

The total phenolics and total flavonoid quantities of JAUN were calculated using the Folin–Ciocalteu colorimetry and the aluminum chloride colorimetry.

### 2.4. DPPH and ABTS Radical Scavenging Activity Assay

The ability of JAUN to eliminate DPPH and ABTS was assessed, wherein 40  $\mu\text{L}$  of the sample was combined with either 40  $\mu\text{L}$  of 0.2 mM DPPH solution or 160  $\mu\text{L}$  of ABTS solution. After mixing, the reaction mixtures were allowed to incubate in darkness for 30 min. As a positive control, ascorbic acid was employed. Subsequently, absorbance was recorded at 520 nm or 405 nm. The amount to which the free radicals DPPH and ABTS were inhibited was calculated using the formula below.

$$\text{DPPH and ABTS scavenging activity(\%)} = \frac{\text{OD}_0 - \text{OD}_x}{\text{OD}_0} \times 100$$

$\text{OD}_0$ : optical density of negative control;  $\text{OD}_x$ : optical density of the sample.

### 2.5. Cell Culture and Photoaging Model Establishment

HaCaT cells were cultivated in the incubator under a humidified 5%  $\text{CO}_2$  and 37  $^\circ\text{C}$  environment. For cell culture, heat-inactivated FBS and antibiotic/antifungal solutions were added to DMEM. For all experiments, HaCaT cells were seeded at a density of  $3 \times 10^6$  cells per 100 mm cell culture dish.

Once the cells achieved 80% confluence, they were subjected to treatment with JAUN in serum-free DMEM. Following an incubation period of 1 h, the cells were subsequently exposed to UVB irradiation at a dosage of 125  $\text{mJ}/\text{cm}^2$  using the Bio-Link BLX-312 (Vilber Lourmat GmbH, Marne-la-Vallée, France).

### 2.6. Cytotoxicity Assay

The MTT assay was employed for cell viability assessment. Following UVB irradiation of the cells, they were incubated with an MTT solution for 4 h. Subsequently, the culture medium was discarded, and a DMSO solution was added, followed by shaking for 30 min to dissolve the formazan crystals.

### 2.7. ROS Inhibitory Activity Assay

Intracellular ROS levels were evaluated in HaCaT cells after 24 h of exposure to UVB irradiation. After discarding the supernatant, the cells were incubated with 30  $\mu\text{M}$  of DCFH-DA for 30 min in a light-free environment. Subsequently, 0.25% trypsin-EDTA was employed to detach the cells. Quantification of intracellular ROS levels was conducted utilizing the BD Accuri C6 flow cytometry system (BD Biosciences, Ann Arbor, MI, USA).

### 2.8. Collagenase and Elastase Inhibition Assay

For the collagenase inhibition assay, buffer A was prepared by dissolving 0.1 M Tris-HCl and 4 mM  $\text{CaCl}_2$  together in distilled water. First, 20  $\mu\text{L}$  of the cell supernatant, 30  $\mu\text{L}$  of 0.2  $\text{mg}/\text{mL}$  collagenase diluted with buffer A, and 50  $\mu\text{L}$  of 0.3  $\text{mg}/\text{mL}$  4-phenylazobenzoyloxycarbonyl-Pro-Leu-Gly-Pro-D-Arg solution were prepared, followed by mixing, after which the reaction was allowed to proceed for 20 min. Subsequently, 100  $\mu\text{L}$  of 6% citric acid and 300  $\mu\text{L}$  of ethyl acetate were added and centrifuged at  $3000 \times g$  for 10 min. The absorption value at the wavelength of 320 nm was then measured.

For the elastase inhibition assay, 50  $\mu\text{L}$  of 0.4 M Tris-HCl buffer was added first, followed by 100  $\mu\text{L}$  of cell supernatant per well and then 50  $\mu\text{L}$  of an enzyme (diluted with 50 mM buffer). The last step was to add 100  $\mu\text{L}$  of 1 mg/mL N-succinyl-Ala-Ala-p-nitroanilide to each well. Elastase concentration was determined by measuring the absorbance at 410 nm after the test had been run at 37 °C for 30 min.

### 2.9. ELISA

We quantitatively assessed the levels of MMP-1 and MMP-3 in the supernatant of the photoaging model using commercially available ELISA reagents. The experimental procedures were conducted in strict accordance with the instructions provided by the reagent manufacturer.

### 2.10. RT-PCR

RNA extraction was performed using TRIzol Reagent (Life Technologies Corporation, CA, USA) as the solvent. For reverse transcription, equimolar amounts of RNA were subjected to reverse transcription using a PCR premix containing both an oligo-(dT)15 primer and a hexamer primer. PCR amplification was carried out using the designated primer pairs listed in Supplementary Table S1 along with the PCR premix. Detection of the amplification products was achieved through nucleic acid staining, followed by visualization using gel electrophoresis under UV illumination. The glyceraldehyde 3-phosphate dehydrogenase (GAPDH) was utilized as a standard for normalizing total mRNA.

### 2.11. Western Blotting

Sensitized cell lysates collected with a spatula were pooled in RIPA buffer and incubated for at least 1 h, followed by centrifugation to isolate total protein extracts. The protein levels have been determined using BCA kits (Thermo Scientific, Rockford, IL, USA). Sodium dodecyl sulfate (SDS)-polyacrylamide gel electrophoresis was used to separate homogenized proteins and then transferred to polyvinylidene fluoride (PVDF) membranes (Bio-Rad Laboratories). The membranes were incubated overnight at 4 °C with primary antibodies, followed by 1 h incubation with secondary antibodies. Chemiluminescence detection was performed using ECL reagents (Marlborough, MA, USA) and analyzed with ImageMaster™ 2D Elite software, version 3.1 (Amersham Pharmacia Biotech, Piscataway, NJ, USA).  $\beta$ -Actin was utilized as a standard for normalizing total protein extracts.

### 2.12. Statistical Analysis

Data were assessed using GraphPad Prism 5 (GraphPad Software Inc., La Jolla, CA, USA), ImageJ (National Institutes of Health, Bethesda, MD, USA), and SigmaPlot 12.0 (Systat Software Inc., San Jose, CA, USA). Statistical significance was set as follows: \*  $p < 0.05$ , \*\*  $p < 0.01$ , and \*\*\*  $p < 0.001$ .

## 3. Results

### 3.1. Identified of JAUN

It was confirmed whether the standard substances of *Lithospermum erythrorhizon*, *Angelica gigas*, and *Scutellaria baicalensis* contained in JAUN were detected. As shown in Figure 1, the retention time of standards at baicalin, shikonin, and decurin were  $8.43 \pm 0.008$ ,  $19.62 \pm 0.006$ , and  $20.37 \pm 0.002$  min, respectively. The baicalin, shikonin, and decurin were identified in JAUN at the retention time of 8.440, 19.610, and 20.373 min, respectively.

### 3.2. Phenolic and Flavonoid Contents of JAUN

The results of the assessment of total phenolic and flavonoid content in JAUN are presented in Table 1. Notably, JAUN exhibited elevated levels of phenolic compounds, with a recorded concentration of  $222.97 \pm 2.37$  mg gallic acid/g extract, as well as abundant flavonoid content, quantified at  $110.14 \pm 0.004$  mg quercetin/g extract.

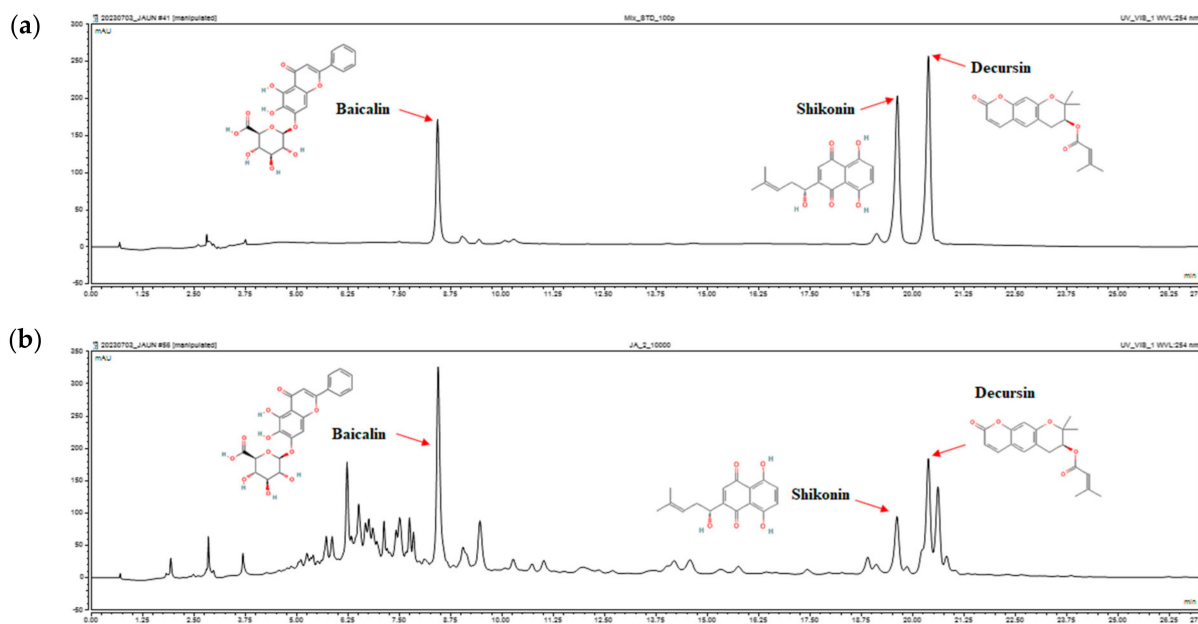


**Figure 1.** HPLC analysis of baicalin, shikonin, and decursin standards (a) and the baicalin, shikonin, and decursin content of JAUN (b).

**Table 1.** Total phenolic and flavonoid contents of JAUN.

	TPC (mg Gallic Acid/g Extract)	TFC (mg Quercetin/g Extract)
JAUN	222.97 ± 2.37	110.14 ± 0.004

Findings are displayed as the mean ± SD from three replicates.

### 3.3. Effect of DPPH and ABTS Radical Scavenging Activity

By assessing the capacity of JAUN to scavenge DPPH and ABTS free radicals, its antioxidative proficiency was initially established. As shown in Figure 2, JAUN exhibited a significant dose-dependent manner in effectively reducing the formation of DPPH and ABTS free radicals. The IC<sub>50</sub> values for DPPH and ABTS free radical scavenging were 155.9 and 183.3 µg/mL, respectively.

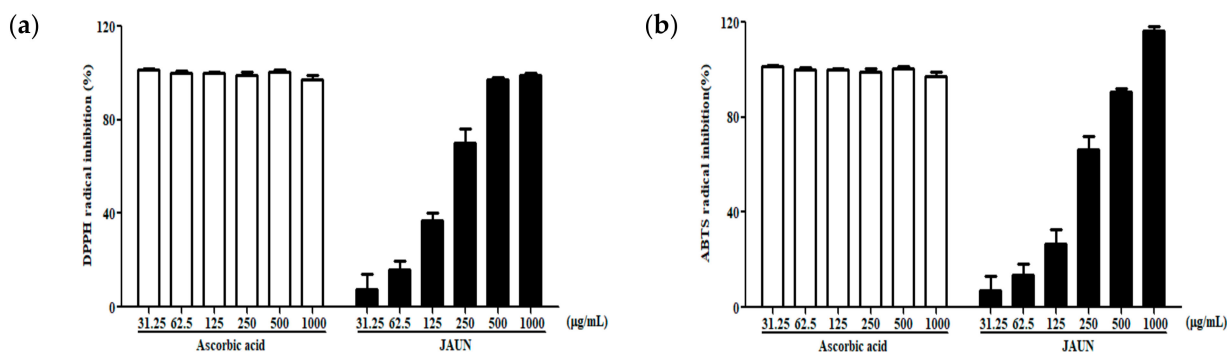


**Figure 2.** Activity of JAUN in scavenging DPPH (a) and ABTS (b) free radicals. Ascorbic acid was used as a positive control. Findings are displayed as the mean ± SD from three replicates.

### 3.4. Cytotoxic Effect of JAUN

Further, 10, 50, and 100 µg/mL JAUN treatments had no considerable toxicity on UVB-irradiated HaCaT cells (Figure 3). This means that these three concentrations of JAUN will not affect the accuracy of the experimental results by causing many cells to die. Based on these results, we chose these as the concentrations for the next experiment.

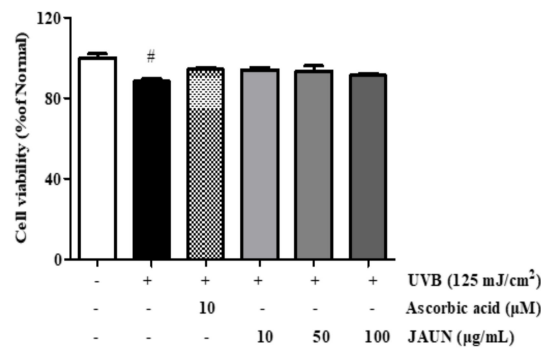


**Figure 3.** Cell viability of photoaging model with or without JAUN. Ascorbic acid was used as a positive control. Findings are displayed as the mean ± SD from three replicates. #  $p < 0.05$  compared with the group only subjected to UVB irradiation.

### 3.5. Effect of JAUN on ROS Generation

As shown in Figure 4, ROS production in HaCaT cells increased by 56.56% following UVB irradiation. The results showed that the administration of JAUN led to a significant and dose-dependent decrease in intracellular ROS levels. Notably, after treatment with JAUN at a concentration of 100 μg/mL, intracellular ROS levels decreased by 35.46%. This reduction rate is higher than the 34.09% observed in the positive control group.

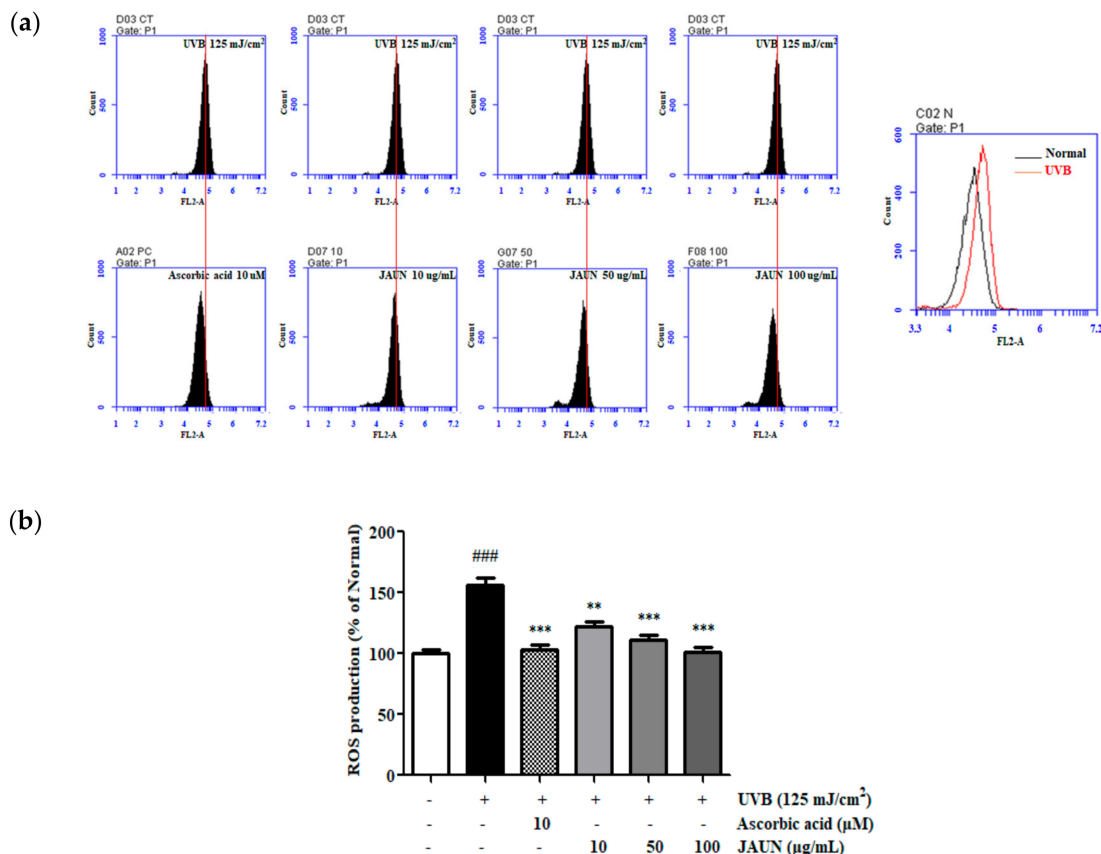


**Figure 4.** JAUN inhibits intracellular ROS levels in photoaging model. A plot of cell number against DCFH-DA detected in the FL-2 channel (a). Results are shown as a histogram (b). Findings are displayed as the mean ± SD from three replicates. <sup>###</sup>  $p < 0.05$  compared with the unirradiated group. <sup>\*\*</sup>  $p < 0.01$ , <sup>\*\*\*</sup>  $p < 0.001$  compared with the group treated only with UVB irradiation.

### 3.6. Effect of JAUN on Collagenase and Elastase Inhibitory Activity

The degree of inhibition of collagenase and elastase by JAUN was ascertained by measuring their activities in the supernatant of HaCaT cells after UVB irradiation. As shown in Figure 5, the dose-dependent inhibition of collagenase and elastase activity by JAUN. Among the obtained results, treatment with 100 µg/mL JAUN successfully inhibited collagenase and elastase activities by 31.39% and 60.88%, respectively.

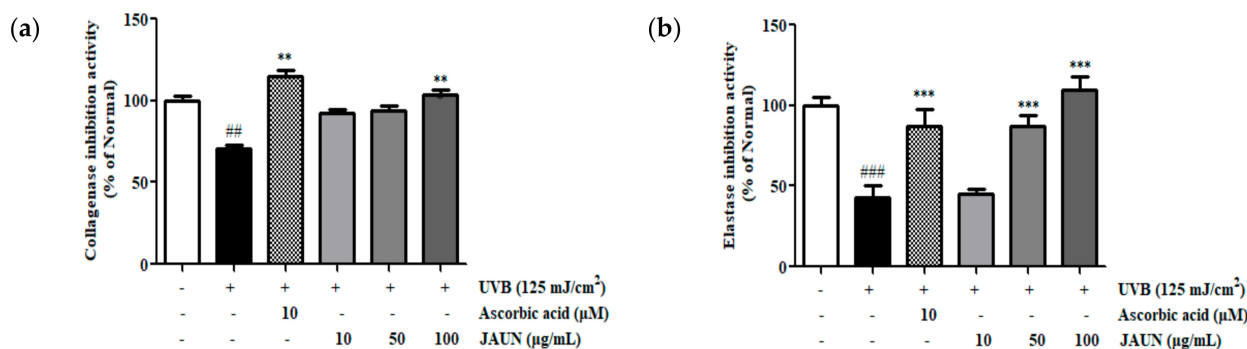


**Figure 5.** Activity of JAUN in inhibiting collagenase (a) and elastase (b) in photoaging model. Findings are displayed as the mean ± SD from three replicates. <sup>##</sup>  $p < 0.01$ , <sup>###</sup>  $p < 0.001$  compared with unirradiated group, <sup>\*\*</sup>  $p < 0.01$ , <sup>\*\*\*</sup>  $p < 0.001$  compared with the group treated only with UVB irradiation.

### 3.7. Effect of JAUN on MMP-1 and MMP-3 Production

MMP-1 and MMP-3 protein levels in UVB-irradiated HaCaT cells exhibited an increase of 83.74% and 60.96%, respectively, as shown in Figure 6. Upon JAUN treatment, there was a decrease in MMP-1 and MMP-3 production, surpassing the reductions observed in the ascorbic acid group. Particularly, the impact of JAUN at a dosage of 100 µg/mL, led to a substantial reduction in MMP-1 and MMP-3 levels of 91.84% and 80.39%, respectively, compared to the levels found in the UVB-irradiated group.

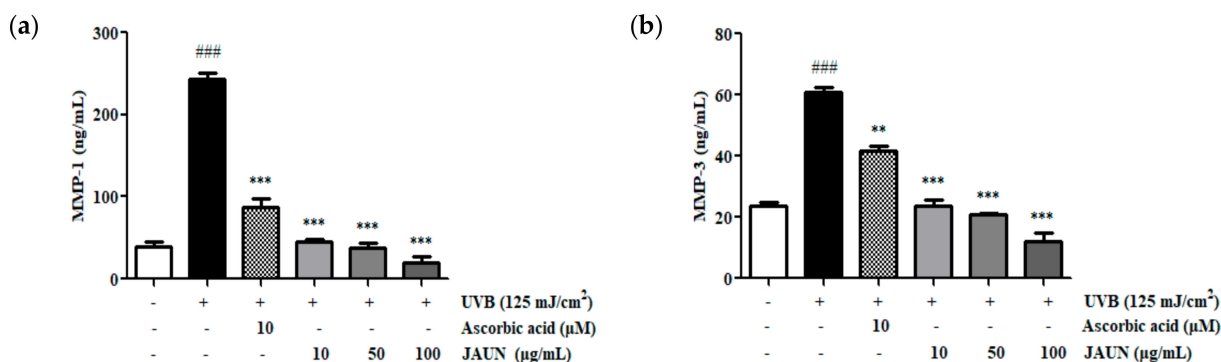


**Figure 6.** JAUN reduces MMP-1 (a) and MMP-3 (b) levels in photoaging model. Findings are displayed as the mean ± SD from three replicates. <sup>###</sup>  $p < 0.001$  compared with the unirradiated group, <sup>\*\*</sup>  $p < 0.01$ , <sup>\*\*\*</sup>  $p < 0.001$  compared with the group treated only with UVB irradiation.

### 3.8. Effect of JAUN on Procollagen Type I, MMP-1, and MMP-3 mRNA Expression

As shown in Figure 7, the mRNA levels of MMP-1 and MMP-3 associated with UVB irradiation exhibited a decrease of 72.33% and 52.50%, respectively, in response to treatment with 100 µg/mL JAUN. Meanwhile, the level of procollagen type I showed a notable increase of 56.68%.

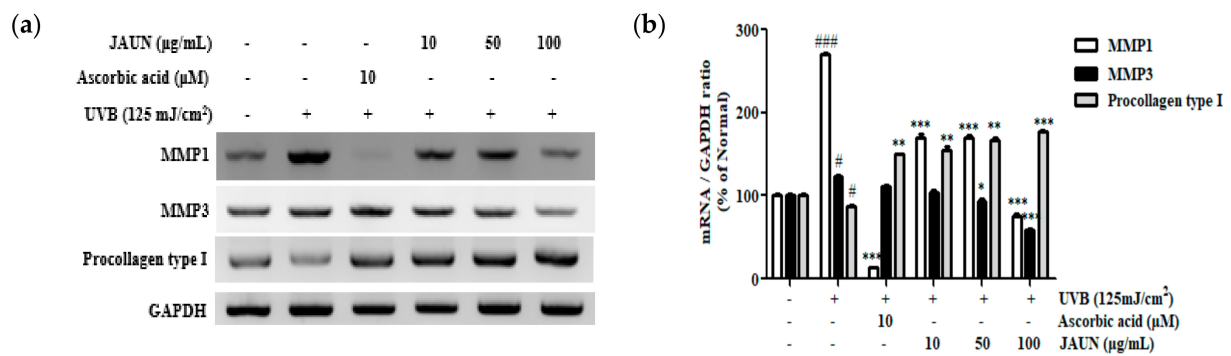


**Figure 7.** The mRNA expression levels of MMP-1, MMP-3, and procollagen type I in photoaging model. MMP-1, MMP-3, and procollagen type I mRNA levels (a) and the band intensities (b). GAPDH mRNA was used as an internal control. Findings are displayed as the mean  $\pm$  SD from three replicates. #  $p < 0.05$ , ###  $p < 0.001$ , compared with unirradiated group; \*  $p < 0.05$ , \*\*  $p < 0.01$ , \*\*\*  $p < 0.001$ , compared with the group treated only with UVB irradiation.

### 3.9. Effect of JAUN on MAPK/AP-1 Signaling Pathway

UVB irradiation upregulated the phosphorylation of members of the MAPK and AP-1 families. Meanwhile, JAUN treatment reversed these changes in a concentration-dependent manner. The application of 100  $\mu\text{g/mL}$  JAUN led to significant suppression of c-Jun and c-fos phosphorylation by 26.92% and 49.25%, respectively, as shown in Figure 8b. Furthermore, JAUN demonstrated a remarkable reduction in the phosphorylation levels of p38, ERK, and JNK by 78.61%, 55.33%, and 71.43%, respectively, at a dosage of 100  $\mu\text{g/mL}$  (Figure 8d).

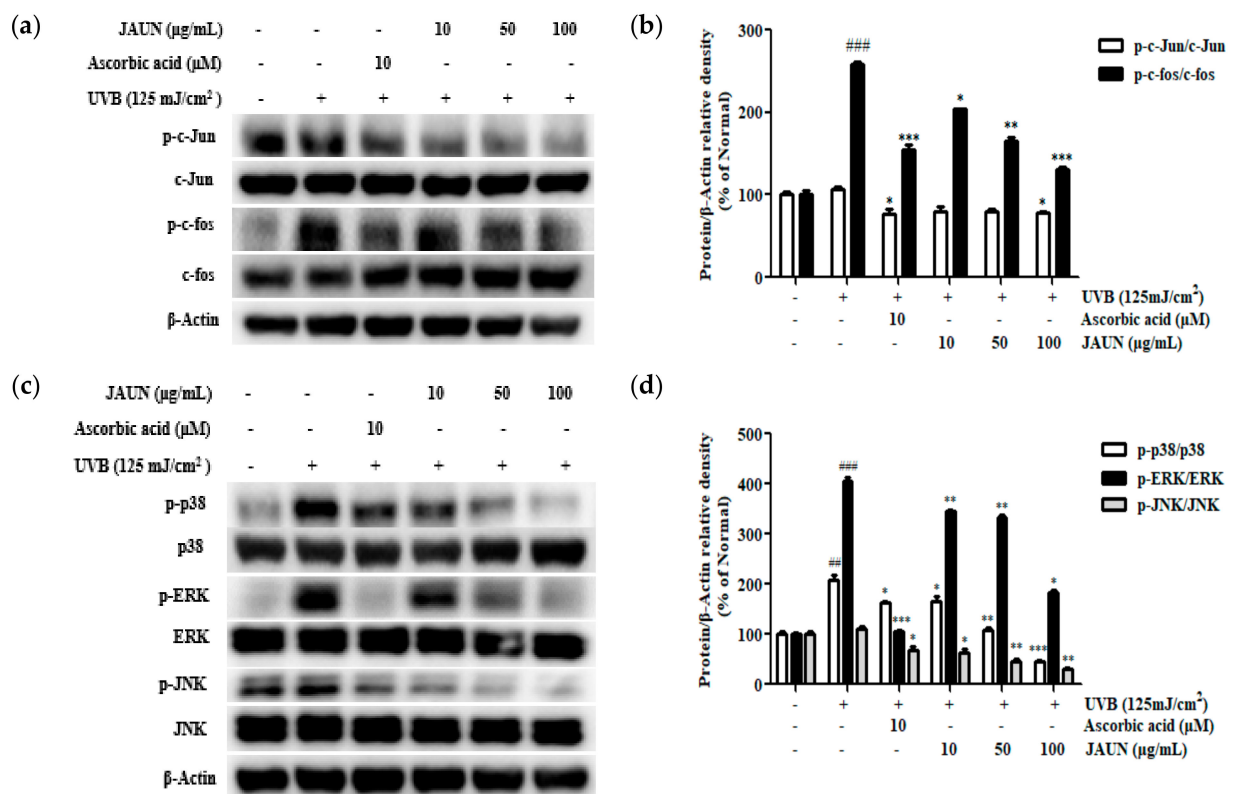


**Figure 8.** JAUN inhibits the phosphorylation levels of MAPK/AP-1 signaling-related proteins in photoaging model. Phosphorylated and unphosphorylated members of the c-Jun and c-fos complex (a); p38, ERK, and JNK (c) protein levels; and the band intensities (b,d).  $\beta$ -Actin was used as an internal

control. Findings are displayed as the mean ± SD from three replicates. ##  $p < 0.01$ , ###  $p < 0.001$  compared with the unirradiated group, \*  $p < 0.05$ , \*\*  $p < 0.01$ , \*\*\*  $p < 0.001$  compared with the group treated only with UVB irradiation.

### 3.10. Effect of JAUN on Nrf2/ARE Signaling Pathway

The impact of JAUN on the Nrf2/ARE antioxidative stress pathway within cells was investigated. The findings unequivocally indicated the successful stimulation of the Nrf2 signaling pathway through JAUN therapy. Following treatment with 100 µg/mL JAUN (Figure 9), there was a notable enhancement in the expression levels of Nrf2, DLD, NQO-1, and HO-1 by 31.93%, 26.78%, 35.32%, and 34.43%, respectively.

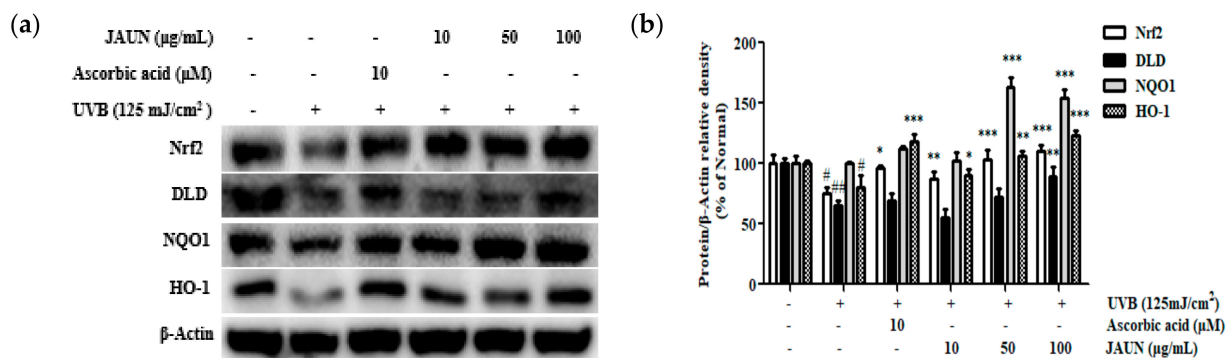


**Figure 9.** JAUN increases the levels of Nrf2/ARE signaling-related proteins in photoaging model. Nrf2, DLD, NQO1, and HO-1 protein levels (a) and band intensities (b). β-Actin was used as an internal control. Findings are displayed as the mean ± SD from three replicates. #  $p < 0.05$ , ##  $p < 0.01$  compared with the unirradiated group; \*  $p < 0.05$ , \*\*  $p < 0.01$ , \*\*\*  $p < 0.001$  compared with the group treated only with UVB irradiation.

### 3.11. Effect of JAUN on TGF-β/Smad7 Signaling Pathway

According to Figure 10, the amount of TGF-β and the phosphorylation rates of Smad2 and Smad3 reduced during UVB irradiation by 79.89%, 28.69%, and 52.61%, respectively. However, compared to unirradiated cells, the level of Smad7 rose by 73.40%. An amount of 100 µg/mL JAUN raised the level of TGF-β, and the phosphorylation levels of Smad2 and Smad3 by 88.32%, 57.17%, and 37.21%, respectively, in comparison to the results in the UVB-irradiated group, while Smad7 dropped by 51.98%.

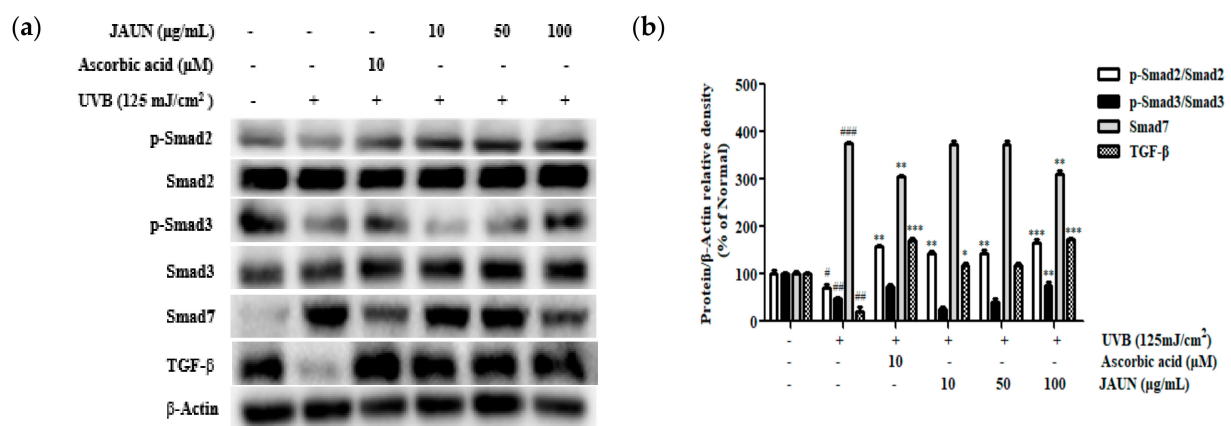


**Figure 10.** JAUN increases the levels of TGF-β/Smad signaling-related proteins in photoaging model. TGF-β, Smad7, phosphorylated and unphosphorylated Smad2/3 protein levels (a) and band intensities (b). β-Actin was used as an internal control. Findings are displayed as the mean ± SD from three replicates. #  $p < 0.05$ , ##  $p < 0.01$ , ###  $p < 0.001$  compared with the unirradiated group; \*  $p < 0.05$ , \*\*  $p < 0.01$ , \*\*\*  $p < 0.001$  compared with the group treated only with UVB irradiation.

#### 4. Discussion

JAUN has been continuously improved and used since the Edo period in Japan, with a history of use exceeding 400 years. Although many recipes for producing JAUN have been developed, *Lithospermum erythrorhizon* and *Angelica gigas* are indispensable. The ingredients in multiple herbal blends often have complementary effects, working together to enhance the therapeutic or other properties of the mixture [21]. This study examined whether JAUN reduces UVB-induced photoaging by modulating the Nrf2/ARE and TGF- $\beta$ /Smad signaling pathways by examining the effects of JAUN therapy on UVB-irradiated HaCaT cells.

ROS are byproducts of the mitochondrial aerobic metabolism electron transfer chain and are regarded as the primary source of intrinsic aging apart from genetic factors [22]. UVB irradiation leads to the overproduction of ROS, accelerating the endogenous aging process, so to confirm the occurrence of anti-photoaging effects, it is necessary to verify changes in ROS. Here, we showed that treatment with 100  $\mu\text{g}/\text{mL}$  JAUN effectively reduced the 35.46% increase in ROS induced by UVB irradiation (Figure 4). Nrf2/ARE is a key player in the protection of the skin against photoaging, and the activation of Nrf2/ARE can coordinate cellular defense mechanisms, including DNA repair, phase II detoxification, antioxidant response, and inflammatory signals [23]. Research by Sun et al. showed that Nrf2/ARE combats ROS by transcriptionally upregulating the expression of detoxifying enzymes and antioxidants, showing an anti-photoaging effect [24]. Therefore, we examined the levels of Nrf2 signaling pathways in UVB-irradiated HaCaT cells to identify Nrf2-related mechanisms controlled by JAUN. Interestingly, the outcomes revealed that the degree of Nrf2 upregulation by 100  $\mu\text{g}/\text{mL}$  JAUN was 1.6 times higher than that of the commonly used anti-photoaging cosmetic additive ascorbic acid (Figure 9).

Reactive oxygen species generation is known to trigger UVB-irradiated induction of MMPs. The zinc-dependent endopeptidases MMPs represent a large class of regulatory proteases in the ECM that is secreted by dermal keratinocytes and are responsible for the degradation of connective tissue and ultimately skin aging [25]. Therefore, inhibiting the secretion of MMPs to alleviate ECM degradation is an effective way of countering photoaging. Recently, *Carica papaya* leaf has been shown to achieve anti-photoaging effects by downregulating the secretion of MMPs [26]. Our results presented in Figures 6 and 7 demonstrate that treatment with JAUN decreases the release of MMP-1 and MMP-3. UVB-induced ROS production activates the MAPK signaling pathway and then stimulates MMP gene transcription by activating the AP-1 transcriptional factor. Therefore, MAPK/AP-1 signaling activation has been thought to play a dominant role in inducing the release of MMP-1. Research by Yang et al. revealed that the MAPK/AP-1 signaling pathway is capable of controlling MMP secretion [27]. The AP-1 complex protein is immediately phosphorylated upon activation of the MAPK signaling pathway, and the AP-1 transcription factor is primarily in charge of controlling MMP production and activity. From the results shown in Figure 8, JAUN also exhibited an excellent effect of downregulating MAPK/AP-1 phosphorylation, which may explain why JAUN downregulates MMPs.

The TGF- $\beta$ /Smad signaling pathway mainly promotes the expression of fibrotic proteins in the ECM, including collagen [28]. By the way, UV irradiation has been suggested to trigger ROS, cause the loss of TGF- $\beta$  receptor expression, and increase Smad 7 expression, which in turn blocks the TGF- $\beta$ /Smad signaling axis. Recently, a study has shown that UVB irradiation can downregulate TGF- $\beta$  expression, but unsaponifiable matter from *Perilla* seed meal reverses this effect [29]. Therefore, we hypothesized that the mechanism of action of JAUN in combating photoaging also includes the TGF- $\beta$ /Smad signaling pathway. As shown in Figure 10, JAUN treatment promoted the R-Smads (Smad2 and Smad3) to phosphorylation, which then oligomerized with common mediator co-Smads to form complexes, migrated into the nucleus, and activated TGF- $\beta$  protein expression to encourage procollagen type I production. Notably, treatments with 100  $\mu\text{g}/\text{mL}$  JAUN and 10  $\mu\text{M}$  ascorbic acid had nearly the same effect in reversing the UVB-induced downregulation of TGF- $\beta$  expression, and 100  $\mu\text{g}/\text{mL}$  JAUN significantly downregulated the signal transduction inhibitor Smad7. Meanwhile, PCR results revealed that procollagen type I

expression was increased by 56.68%, which is far better than the 1.6 fold restoration effect of ascorbic acid (Figure 7). Overall, our results support the use of JAUN to prepare skincare products for repairing and regenerating key proteins in photodamaged skin.

## 5. Conclusions

In this study, we successfully revealed the mechanism by which JAUN protects against UVB-induced photoaging of HaCaT cells at the molecular level. Specifically, treatment with JAUN at a high concentration effectively restored the expression of the Nrf2/ARE pathway in HaCaT cells after UVB irradiation, downregulated MAPK/AP-1 phosphorylation, reduced ROS, and successfully downregulated MMP-1 and MMP-3. At the same time, it also promoted Smad2 and 3 phosphorylation, decreased Smad7 expression, and effectively increased TGF- $\beta$  expression. Finally, it effectively promoted the synthesis of procollagen type I and prevented ECM quenching caused by UVB irradiation. This study provides insights that can guide the future development of JAUN as a cosmetic additive to combat skin photoaging caused by UVB irradiation. However, one limitation of this study is its focus on demonstrating the anti-photoaging effects of JAUN solely through in vitro cell experiments. Further research is required to explore its clinical applications. Additionally, JAUN exhibits potent antioxidant effects in addition to its anti-photoaging properties, suggesting potential applications for addressing other conditions linked to oxidative stress.

**Supplementary Materials:** The following supporting information can be downloaded at: <https://www.mdpi.com/article/10.3390/app131810425/s1>, Table S1. Primers used for RT-PCR.

**Author Contributions:** Conceptualization, T.-H.Y., H.K. and S.O.; methodology, S.O. and Q.Z.; software, Q.Z. and M.K.; validation, H.K. and S.O.; formal analysis, Q.Z., S.O. and S.Z.; investigation, T.-H.Y., H.K. and S.O.; resources, H.K. and S.Z.; data curation, S.O. and S.Z.; writing—Q.Z. and S.O.; writing—review and editing, Q.Z. and S.O.; visualization, M.K. and S.Z.; supervision, T.-H.Y.; project administration, T.-H.Y. All authors have read and agreed to the published version of the manuscript.

**Funding:** This research was funded by Kyung Hee University, grant number 20230860.

**Institutional Review Board Statement:** Not applicable.

**Informed Consent Statement:** Not applicable.

**Data Availability Statement:** The data presented in this study are available in this paper.

**Acknowledgments:** This work was supported by J1 Cosbio Co., Ltd.

**Conflicts of Interest:** The authors declare no conflict of interest.

## References

1. Reich, A.; Mędrak, K. Effects of narrow band UVB (311 nm) irradiation on epidermal cells. *Int. J. Mol. Sci.* **2013**, *14*, 8456–8466. [[CrossRef](#)]
2. Rabe, J.H.; Mamelak, A.J.; McElgunn, P.J.; Morison, W.L.; Sauder, D.N. Photoaging: Mechanisms and repair. *J. Am. Acad. Dermatol.* **2006**, *55*, 1–19. [[CrossRef](#)] [[PubMed](#)]
3. Sherratt, M.J.; Bayley, C.P.; Reilly, S.M.; Gibbs, N.K.; Griffiths, C.E.; Watson, R.E. Low-dose ultraviolet radiation selectively degrades chromophore-rich extracellular matrix components. *J. Pathol.* **2010**, *222*, 32–40. [[CrossRef](#)]
4. Watson, R.E.; Gibbs, N.K.; Griffiths, C.E.; Sherratt, M.J.; Haselhuhn, A.S.; Gooding, E.J.; Glover, A.G.; Anzalone, G.C.; Wijnen, B.; Sanders, P.G.; et al. Damage to skin extracellular matrix induced by UV exposure. *Antioxid. Redox Signal.* **2014**, *21*, 1063–1077. [[CrossRef](#)] [[PubMed](#)]
5. Schieber, M.; Chandel, N.S. ROS function in redox signaling and oxidative stress. *Curr. Biol.* **2014**, *24*, R453–R462. [[CrossRef](#)]
6. Srinivas, U.S.; Tan, B.W.Q.; Vellayappan, B.A.; Jeyasekharan, A.D. ROS and the DNA damage response in cancer. *Redox Biol.* **2019**, *25*, 101084. [[CrossRef](#)]
7. Hemnani, T.; Parihar, M.S. Reactive oxygen species and oxidative DNA damage. *Indian J. Physiol. Pharmacol.* **1998**, *42*, 440–452. [[PubMed](#)]
8. Kim, J.-M.; Kim, S.Y.; Noh, E.-M.; Song, H.-K.; Lee, G.-S.; Kwon, K.-B.; Lee, Y.-R. Reversine inhibits MMP-1 and MMP-3 expressions by suppressing of ROS/MAPK/AP-1 activation in UV-stimulated human keratinocytes and dermal fibroblasts. *Exp. Dermatol.* **2018**, *27*, 298–301. [[CrossRef](#)]

9. Hwang, E.; Ngo, H.T.; Seo, S.A.; Park, B.; Zhang, M.; Yi, T.H. Protective effect of dietary *Alchemilla mollis* on UVB-irradiated premature skin aging through regulation of transcription factor NFATc1 and Nrf2/ARE pathways. *Phytomedicine* **2018**, *39*, 125–136. [[CrossRef](#)]
10. Zhang, M.; Hwang, E.; Lin, P.; Gao, W.; Ngo, H.T.; Yi, T.-H. *Prunella vulgaris* L. exerts a protective effect against extrinsic aging through NF- $\kappa$ B, MAPKs, AP-1, and TGF- $\beta$ /Smad signaling pathways in UVB-aged normal human dermal fibroblasts. *Rejuvenation Res.* **2018**, *21*, 313–322. [[CrossRef](#)]
11. Saha, S.; Buttari, B.; Panieri, E.; Profumo, E.; Saso, L. An overview of Nrf2 signaling pathway and its role in inflammation. *Molecules* **2020**, *25*, 5474. [[CrossRef](#)] [[PubMed](#)]
12. Kim, C.-R.; Kim, Y.-M.; Lee, M.-K.; Kim, I.-H.; Choi, Y.-H.; Nam, T.-J. Pyropia yezoensis peptide promotes collagen synthesis by activating the TGF- $\beta$ /Smad signaling pathway in the human dermal fibroblast cell line Hs27. *Int. J. Mol. Med.* **2016**, *39*, 31–38. [[CrossRef](#)]
13. Afrakhte, M.; Morén, A.; Jossan, S.; Itoh, S.; Sampath, K.; Westermarck, B.; Heldin, C.-H.; Heldin, N.-E.; Heldin, C.-H.; Heldin, N.-E.; et al. Induction of inhibitory Smad6 and Smad7 mRNA by TGF- $\beta$  family members. *Biochem. Biophys. Res. Commun.* **1998**, *249*, 505–511. [[CrossRef](#)] [[PubMed](#)]
14. Choi, M.S.; Yoo, M.S.; Son, D.J.; Jung, H.Y.; Lee, S.H.; Jung, J.K.; Lee, B.C.; Yun, Y.P.; Pyo, H.B.; Hong, J.T. Increase of collagen synthesis by obovatol through stimulation of the TGF- $\beta$  signaling and inhibition of matrix metalloproteinase in UVB-irradiated human fibroblast. *J. Dermatol. Sci.* **2007**, *46*, 127–137. [[CrossRef](#)]
15. Chen, X.; Yang, L.; Oppenheim, J.J.; Howard, O.M.Z. Cellular pharmacology studies of shikonin derivatives. *Phytother. Res.* **2002**, *16*, 199–209. [[CrossRef](#)] [[PubMed](#)]
16. Yoo, H.G.; Lee, B.H.; Kim, W.; Lee, J.S.; Kim, G.H.; Chun, O.K.; Koo, S.I.; Kim, D.-O. *Lithospermum erythrorhizon* extract protects keratinocytes and fibroblasts against oxidative stress. *J. Med. Food* **2014**, *17*, 1189–1196. [[CrossRef](#)]
17. Kim, T.W. Nodakenin induces ROS-dependent apoptotic cell death and ER stress in radioresistant breast cancer. *Antioxidants* **2023**, *12*, 492. [[CrossRef](#)]
18. Oh, J.M.; Lee, H.-S.; Baek, S.C.; Lee, J.P.; Jeong, G.S.; Paik, M.-J.; Kim, H. Antidepressant-like activities of hispidol and decursin in mice and analysis of neurotransmitter monoamines. *Neurochem. Res.* **2020**, *45*, 1930–1940. [[CrossRef](#)]
19. Park, J.Y.; Kwak, J.H.; Kang, K.S.; Jung, E.B.; Lee, D.-S.; Lee, S.; Jung, Y.; Kim, K.H.; Hwang, G.S.; Lee, H.L.; et al. Wound healing effects of deoxyshikonin isolated from Jawoongo: In vitro and in vivo studies. *J. Ethnopharmacol.* **2017**, *199*, 128–137. [[CrossRef](#)]
20. Ku, J.M.; Hong, S.H.; Kim, S.R.; Choi, H.-S.; Kim, H.I.; Kim, D.U.; Oh, S.M.; Seo, H.S.; Kim, T.Y.; Shin, Y.C.; et al. The prevention of 2,4-dinitrochlorobenzene-induced inflammation in atopic dermatitis-like skin lesions in BALB/c mice by Jawoongo. *BMC Complement. Altern. Med.* **2018**, *18*, 215. [[CrossRef](#)]
21. De Smet, P.A. Herbal remedies. *N. Engl. J. Med.* **2002**, *347*, 2046–2056. [[CrossRef](#)] [[PubMed](#)]
22. Detienne, G.; De Haes, W.; Mergan, L.; Edwards, S.L.; Temmerman, L.; Van Bael, S. Beyond ROS clearance: Peroxiredoxins in stress signaling and aging. *Ageing Res. Rev.* **2018**, *44*, 33–48. [[CrossRef](#)] [[PubMed](#)]
23. Xian, D.; Xiong, X.; Xu, J.; Xian, L.; Lei, Q.; Song, J.; Zhong, J. Nrf2 overexpression for the protective effect of skin-derived precursors against UV-induced damage: Evidence from a three-dimensional skin model. *Oxid. Med. Cell. Longev.* **2019**, *2019*, 7021428. [[CrossRef](#)]
24. Sun, Z.; Park, S.Y.; Hwang, E.; Park, B.; Seo, S.A.; Cho, J.-G.; Zhang, M.; Yi, T.-H. Dietary *Foeniculum vulgare* Mill extract attenuated UVB irradiation-induced skin photoaging by activating of Nrf2 and inhibiting MAPK pathways. *Phytomedicine* **2016**, *23*, 1273–1284. [[CrossRef](#)] [[PubMed](#)]
25. Cui, N.; Hu, M.; Khalil, R.A. Biochemical and biological attributes of matrix metalloproteinases. *Prog. Mol. Biol. Transl. Sci.* **2017**, *147*, 1–73. [[PubMed](#)]
26. Seo, S.A.; Ngo, H.T.T.; Hwang, E.; Park, B.; Yi, T.-H. Protective effects of *Carica papaya* leaf against skin photodamage by blocking production of matrix metalloproteinases and collagen degradation in UVB-irradiated normal human dermal fibroblasts. *S. Afr. J. Bot.* **2020**, *131*, 398–405. [[CrossRef](#)]
27. Yang, B.; Ji, C.; Chen, X.; Cui, L.; Bi, Z.; Wan, Y.; Xu, J. Protective effect of astragaloside IV against matrix metalloproteinase-1 expression in ultraviolet-irradiated human dermal fibroblasts. *Arch. Pharm. Res.* **2011**, *34*, 1553–1560. [[CrossRef](#)]
28. Zhao, D.; Shi, Y.; Dang, Y.; Zhai, Y.; Ye, X. Daidzein stimulates collagen synthesis by activating the TGF- $\beta$ /smad signal pathway. *Australas. J. Dermatol.* **2014**, *56*, e7–e14. [[CrossRef](#)]
29. Lee, H.; Sung, J.; Kim, Y.; Jeong, H.S.; Lee, J. Protective effects of unsaponifiable matter from perilla seed meal on UVB-induced damages and the underlying mechanisms in human skin fibroblasts. *Antioxidants* **2019**, *8*, 644. [[CrossRef](#)]

**Disclaimer/Publisher’s Note:** The statements, opinions and data contained in all publications are solely those of the individual author(s) and contributor(s) and not of MDPI and/or the editor(s). MDPI and/or the editor(s) disclaim responsibility for any injury to people or property resulting from any ideas, methods, instructions or products referred to in the content.